



ELSEVIER

Journal of Power Sources 92 (2001) 70–80

JOURNAL OF  
POWER  
SOURCES

www.elsevier.com/locate/jpowersour

# Electrochemical properties of Li–Mg alloy electrodes for lithium batteries

Zhong Shi<sup>a</sup>, Meilin Liu<sup>a,\*</sup>, Devang Naik<sup>b</sup>, James L. Gole<sup>b,1</sup><sup>a</sup>*School of Materials Science and Engineering, Georgia Institute of Technology, Atlanta, GA 30332, USA*<sup>b</sup>*School of Physics, Georgia Institute of Technology, Atlanta, GA 30332, USA*

Received 12 February 2000; accepted 16 May 2000

## Abstract

Li–Mg alloy electrodes are prepared by two methods: (1) direct-alloying through the melting of mole percent specific mixtures of Li and Mg metal under vacuum and (2) the kinetically-controlled vapor formation and deposition (KCVD) of a Li–Mg alloy on a substrate. It is found that processing conditions greatly influence the microstructures and surface morphologies, and hence, the electrochemical properties of the Li–Mg alloy electrodes. When applying the KCVD technique, the composition of each prepared alloy is determined by independently varying the temperature of the molten lithium, the temperature of magnesium with which the lithium interacts, and the temperature of the substrate on which the intimately mixed Li–Mg mixture is deposited. Here, the required temperature for lithium induced Mg vaporization is more than 200°C below the magnesium melting point. The effect of these variable temperatures on the microstructure, morphology, and electrochemical properties of the vapor-deposited alloys has been studied. The diffusion coefficients for lithium in the Li–Mg alloy electrodes prepared by the KCVD method are in the range  $1.2 \times 10^{-7}$  to  $5.2 \times 10^{-7}$  cm<sup>2</sup> s<sup>-1</sup> at room temperature, two to three orders of magnitude larger than those in other lithium alloy systems (e.g.  $6.0 \times 10^{-10}$  cm<sup>2</sup> s<sup>-1</sup> in LiAl). These observations suggest that Li–Mg alloys prepared by the KCVD method might be used effectively to prevent dendrite formation, improving the cycleability of lithium electrodes and the rechargeability of lithium batteries as a result of the high diffusion coefficient of lithium atoms in the Li–Mg alloy. Li–Mg alloy electrodes also appear to show not only the potential for higher rate capabilities (power densities) but also for larger capacities (energy densities) which might considerably exceed those of lithiated carbon or Sn-based electrodes for lithium batteries. © 2001 Elsevier Science B.V. All rights reserved.

**Keywords:** Lithium–magnesium alloy; Kinetically-controlled vapor deposition; Electrochemical behavior; Lithium diffusion; Lithium battery

## 1. Introduction

While the high activity of lithium makes it attractive as a unique energy source for microelectronic devices, a critical issue plaguing existing lithium batteries is the cycleability of the lithium electrodes, and hence, the rechargeability of the battery system. The formation of a dendritic structure during charging is one of the major problems associated with pure lithium used as the negative electrode in a secondary lithium battery. Typically, dendrite growth worsens progressively during cycling, often leading to both disconnection and electrical isolation of the active lithium or electrical shorting between the electrodes. Lithium intercalation materials, such as lithiated carbon, LiAl alloys, and Sn-based composite oxides, have been studied to replace pure lithium in an

effort to reduce the tendency for lithium dendrite formation. In principle, lithium dendrite formation can be avoided as long as the activity of lithium at the electrode–electrolyte interface is kept less than unity. To date, the most widely-studied lithium intercalation materials are various forms of carbon. However, other elements that also form alloys with lithium, including Sn, Pb, Zn, Cd, Mg, Bi, Sb, and As, may represent viable candidates for an efficient alloy battery system.

While carbon-based intercalation compounds have a capacity limited to a theoretical value of 370 mAh g<sup>-1</sup>, corresponding to the reversible insertion–extraction of one lithium atom per six carbon atoms, they also suffer from a significant irreversible capacity loss during the first cycle. In addition to the low capacity inherent to lithiated carbon electrodes, it is also appropriate to consider their rate capability. The reported diffusivity of lithium in Li<sub>x</sub>C<sub>6</sub> at 25°C varies from 10<sup>-8</sup> to 10<sup>-9</sup> cm<sup>2</sup> s<sup>-1</sup>, decreasing linearly with lithium insertion [1], while the reported diffusivity of lithium in Li<sub>7</sub>Sn<sub>3</sub> at 25°C is 3 × 10<sup>-7</sup> to 5 × 10<sup>-7</sup> cm<sup>2</sup> s<sup>-1</sup> [2]. Clearly, the diffusivity of lithium in this lithium alloy is

\* Corresponding author. Tel.: +1-404-894-6114; fax: +1-404-894-9140.

E-mail addresses: meilin.liu@mse.gatech.edu (M. Liu), james.gole@physics.gatech.edu (J.L. Gole).

<sup>1</sup> Co-corresponding author. Tel.: +1-404-894-4029; fax: +1-404-894-9140.

much greater (more than one order of magnitude) than that of the lithiated carbon electrode, implying that lithium alloy electrodes can be charged or discharged at a much higher rate, and hence, batteries based on lithium alloy electrodes will have a much higher power density. It is not surprising, therefore, to find that select extensions to the lighter lithium alloy systems have been considered with the greatest focus being on the Li–Al system. While the historical reasons for this substantial effort on the Li–Al system have been considered by others [3,14,15], we suggest that the Li–Mg system represents a superior alternative. Although most Li–Al alloy electrodes studied (both at high temperatures or in ambient-temperature rechargeable cells) disintegrate or otherwise degrade during cycling due to changes associated with inevitable phase transformations [4], carefully-designed Li–Mg alloy electrodes are expected to have and maintain much better structural and microstructural integrity and stability due to the minimal phase change which they undergo.

In the Li–Al system, each phase is either a line compound or a solid solution with a very narrow range of composition. As a result, electrodes based on Li–Al alloys (of reasonable capacity) must undergo phase transformations during cycling and it is not surprising to see that these electrodes disintegrate or degrade in performance during the cycling. In fact, we have observed severe degradation and even disintegration of Li–Al films containing in excess of 3 wt.% lithium [5]. In stark contrast, the Li–Mg system is fundamentally different from the Li–Al system. Shown in Fig. 1 is the Li–Mg phase diagram [6]. In this system, the Li-rich

solid solution phase ( $\beta$ ) covers almost 90% of the phase diagram; the lithium content of the  $\beta$ -phase in the Li–Mg system varies from about 11 to 100 wt.% (30–100 at.%). Thus, there will be no phase transformation when an electrode in this system is cycled over a wide range of composition (about 89 wt.% change in Li). Within this framework, when an electrode is cycled from  $\text{Li}_4\text{Mg}_6$  to  $\text{Li}_6\text{Mg}_4$  (only about 16.7 wt.% change in Li) the capacity can be  $642 \text{ mAh g}^{-1}$ , which is almost twice the capacity of a lithiated carbon electrode. When the amount of Li inserted into or taken away from a Li–Mg electrode is sufficiently small, it is anticipated that the electrode reaction may, at least in part, correspond to a topotactic or intercalation process. In other words, the Mg in the alloy is expected to function as a frame to maintain the essential topological features of the porous electrode. Accordingly, changes in the structure and microstructure of the alloy electrode, if any, are expected to be minimal during cycling. The degree to which the topological features will be preserved during cycling is yet to be determined; however, it is apparent that the ability of magnesium to take up lithium in alloy is vastly superior to aluminum.

Although various lithium alloys have been studied for high temperature Li/Fe<sub>x</sub>S systems [7,8], few studies have been done on lithium alloy electrodes for ambient temperature batteries. As we have noted, the diffusivities of lithiated carbon electrodes can be starkly contrasted to lithium alloy diffusivities. The reported diffusivity of lithium in the  $\beta$ -phase of a Li–Mg alloy at  $420^\circ\text{C}$  is about  $1.8 \times 10^{-6}$  to  $5 \times 10^{-6} \text{ cm}^2 \text{ s}^{-1}$  [9], suggesting a significant diffusivity at

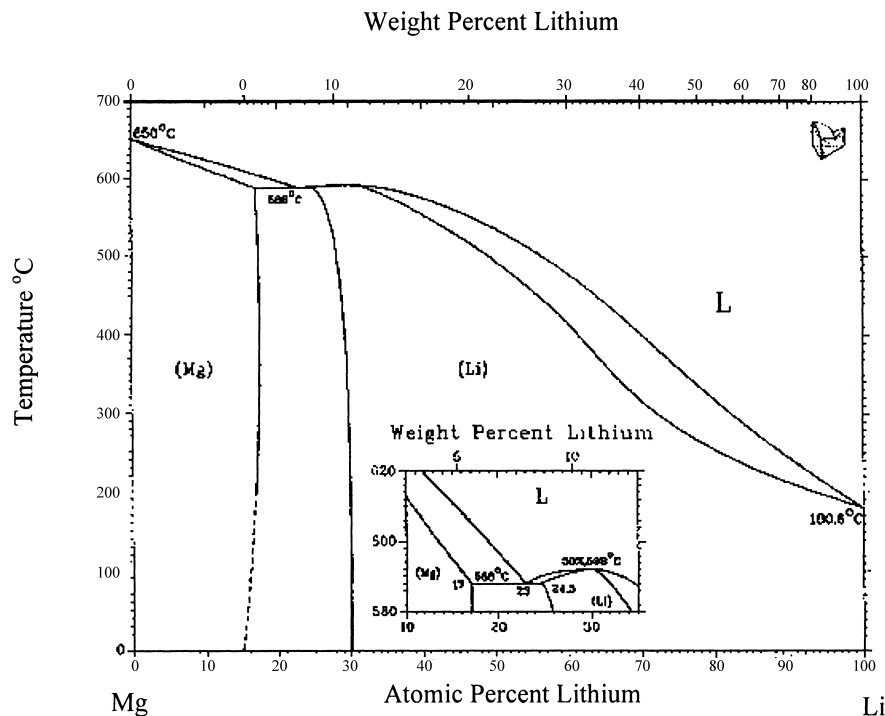


Fig. 1. Equilibrium phase diagram for the Mg–Li system [6].

room temperature which we confirm in this study. Therefore, the dendrite formation to which we have alluded might be avoided. In this paper, we report our initial findings on investigations into the electrochemical properties of Li–Mg alloy electrodes prepared using two contrasting methods.

## 2. Experimental

Pure magnesium powder and lithium rod were purchased from Alfa Inorganics. Magnesium rod stock (1 in. diameter, >98%) was purchased from A.D. Mackey. Definite compositions of Li–Mg alloys were made by mixing predetermined quantities of pure Li metal and Mg powder and heating these mixtures to temperature between 650 and 750°C under vacuum for 3 h in the specially designed container schematically shown in Fig. 2(a). The alloys were then transferred under vacuum to a glove-box (Vacuum Atmospheres Company). Four alloy samples, with the composition of Mg prepared at 10, 20, 30, and 40 wt.% were studied in this work.

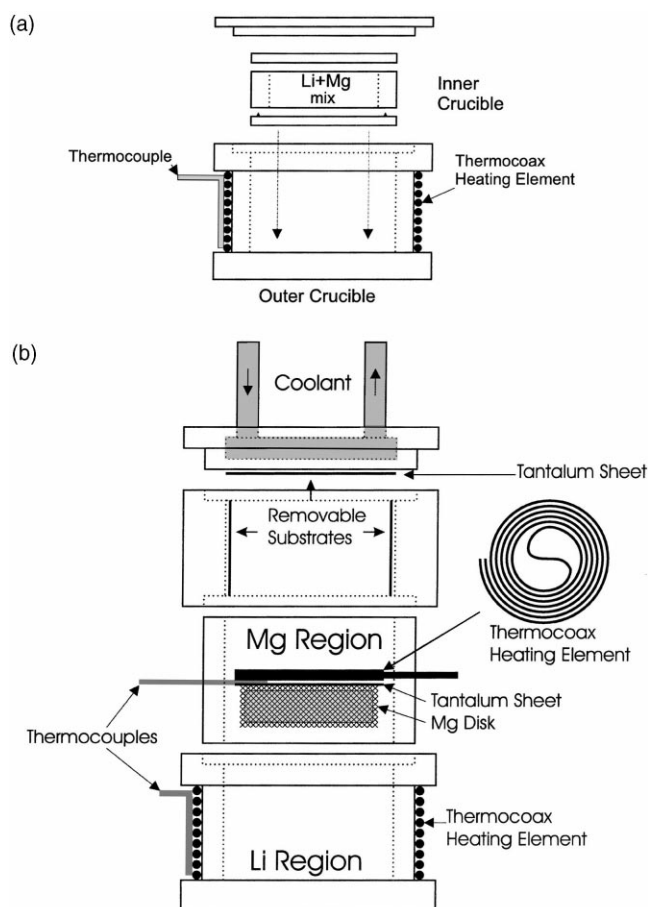


Fig. 2. Schematic configurations for forming Mg–Li alloys by (a) direct-alloying from Mg and Li powders in a closed containment vessel under vacuum at high temperature and (b) kinetically-controlled vapour formation and deposition (KCVD).

The container used for direct-alloying, as depicted in Fig. 2(a), is a double crucible design constructed from 304 stainless steel. The lithium metal–powdered magnesium sample is placed in the inner crucible whose removable bottom is sealed by a knife edge and titanium gasket combination. The top of the inner crucible is held tightly in place by a lock-screw configuration tightened from the outside of the outer heating crucible. After the prepared sample and inner crucible are installed and sealed, the entire configuration is placed in the vacuum chamber which we have previously described [5] at  $10^{-6}$  Torr and the entire device is heated, over a period of several hours to temperatures in excess of 650°C. The outside of the vessel, which is wrapped in thermal coax (Phillips) can readily be heated to temperatures exceeding 700°C as monitored with a thermocouple (Omega type K) placed directly between a tantalum outer sheath and the thermal coax.

The configuration used for the KCVD process, as depicted in Fig. 2(b), represents an improved modification of our previous design [5]. Here, lithium vapor, heated in a lower ‘crucible’ (again with thermal coax) is made to interact with an independently heated magnesium disk (cut from 1 in. rod stock, A.D.Mackey) promoting the controlled liberation of magnesium at temperatures far below its melting point, 651°C. The magnesium disk is mounted to a second thermal coax heating element as the entire grouping (see Fig. 2(b)) is mounted in a second intermediate chamber above the lithium crucible. This configuration facilitates the intimate mixing of magnesium and lithium vapor and promotes the simultaneous vapor deposition of a controlled and intimately mixed magnesium and lithium concentration onto a substrate in the upper crucible region to form a desired magnesium–lithium alloy. The method is to be contrasted with magnesium–lithium vapor deposition systems where separate sources are used for each metal in the alloy. The unique process leading to alloy formation, results in the creation of a significant magnesium vapor at temperatures nearly 200°C (Table 1) below the magnesium melting temperature and is facilitated by the interaction of lithium vapor with the solid magnesium disk [5]. The interlocking containment vessels in Fig. 2(b) are constructed from 304 stainless steel. The upper chamber houses the substrates on which the intimate mix of lithium and magnesium can be deposited both to a tantalum sheet held in place next to a water or dry ice–methanol slush bath cooled top plate or to a tantalum sheet which sheaths and is intimately connected to the inner side walls of the upper chamber.

The outside of the lower lithium containing vessel is wrapped in thermal coax (Phillips) and is usually heated to temperatures exceeding 500°C. Lithium rod placed in the bottom of this container is melted as the container temperature is monitored by a thermocouple (Omega type K) again placed directly next to the thermal coax. The magnesium metal disk/0.005 in. tantalum sheet/heating coil/thermocouple configuration is suspended inside the intermediate

Table 1

Summary of representative experimental conditions for Li–Mg alloy formation using the kinetically controlled vapor deposition method and diffusivity of Li in the alloys as determined using chronoamperometry

Sample number	Mg temperature (°C)	Li temperature (°C)	Substrate temperature (°C)	Diffusion coefficient ( $10^{-7} \text{ cm}^2 \text{ s}^{-1}$ )
1	525	625	~30	1.22
2	485	635	~30	1.8
3	485	635	~15	3.91
4	460	650	~15	5.17

containment vessel as indicated in the figure. The lithium vapor interacts with the magnesium metal and is mixed with the resulting vaporizing magnesium. This mixture can then be made to condense onto the temperature controlled substrate region indicated in the figure. The magnesium and lithium are maintained at two different temperatures (Table 1) using the two control loops of an Omega CN3000 temperature controller. The lithium vapor pressure at the temperature of these experiments ranges from  $\sim 10^{-3}$  to  $10^{-2}$  Torr. The composition of the deposited alloy can be controlled by independently adjusting the magnesium and lithium temperatures.

The experiments on the magnesium–lithium system demonstrate that the presence of lithium vapor appears to enhance the escaping tendency of the surface magnesium metal, and as a result, facilitates the intimate mixing of magnesium and lithium vapors [5]. The effect typically results in the complete vaporization of the magnesium disk in less than 2 h at temperatures in the range of  $450^\circ\text{C}$  (Table 1) [5]. In contrast, in the absence of alkali metal vapors, the magnesium disk remains virtually intact over an identical temperature range. By virtue of the manner in which the magnesium vapor is formed and mixed with lithium vapor, the alloy subsequently deposited on the temperature-controlled substrate can be shown to have a nearly uniform composition. The control of deposition and uniformity of composition clearly distinguishes the process from a codeposition using two beams from independently heated metal sources. The microstructure and surface morphology of the Li–Mg alloys were characterized using a scanning electron microscope (SEM, Hitachi S-800) and the compositions of the alloys were determined (wt.% of lithium) using Inductively Coupled Plasma-Atomic Absorption Spectroscopy (ICP-AAS).

A three-electrode electrochemical cell was employed for the electrochemical measurements presented in this work. The reference and the counter electrode were made of lithium foil and 1 M  $\text{LiN}(\text{SO}_2\text{CF}_3)_2\text{-EC/DMC}$  (1:2 by vol.) solution was used as the electrolyte. The apparent surface area of the alloy electrodes is  $0.2 \text{ cm}^2$ . Two layers of Celgard<sup>®</sup> 2400 film were chosen as the separators. The EC and DMC were dried for at least 24 h with activated 4A molecular sieves. Cyclic voltammetry and chrono-amperometry were performed using a Solatron 1285 system controlled using a personal computer.

### 3. Results and discussion

#### 3.1. Deposition and stripping of Li on Pt and Mg electrode

Shown in Fig. 3 are the cyclic voltammograms (CVs) of a platinum electrode in 1 M  $\text{LiN}(\text{SO}_2\text{CF}_3)_2\text{-EC/DMC}$  (1:2 by vol.) at a scan rate of  $1 \text{ mV s}^{-1}$  for the first five cycles. It is known that Pt alloys with Li [10] and initially, therefore, some of the Li will diffuse into the Pt electrode and will not be available for stripping. Once the interior is saturated with Li, more of the plated Li can be stripped in subsequent cycles, as clearly seen in Fig. 3. There are two oxidation peaks corresponding to Li metal stripping and the extraction of Li from the Li–Pt alloy. It is important to note that the anodic peak current increased with cycle number, indicating that the active surface area of the electrode was increasing, due possibly to the formation of lithium dendrite on the Pt electrode during Li deposition. The shape of the cathodic current responses further supports this: the cathodic current crossover is an indication of an increasing active electrode area during the potential sweep.

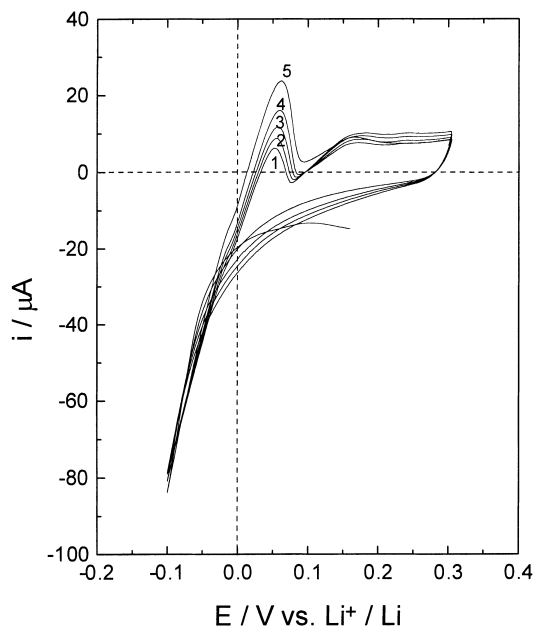


Fig. 3. Cyclic voltammograms of a platinum electrode in 1 M  $\text{LiN}(\text{CF}_3\text{SO}_2)_2\text{-EC/DMC}$  (1:2 by vol.) with a scan rate of  $1 \text{ mV s}^{-1}$ . The number by each CV curve represents the number of the cycle.

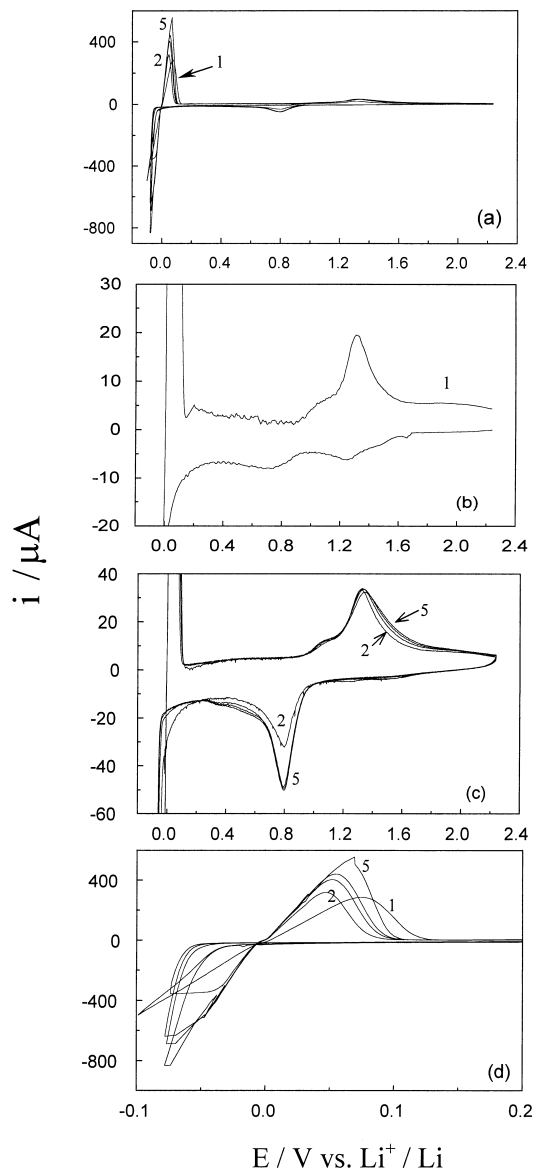


Fig. 4. Cyclic voltammograms of a pure Mg electrode in 1 M LiN(CF<sub>3</sub>SO<sub>2</sub>)<sub>2</sub>-EC/DMC (1:2 by vol.) with a scan rate of 1 mV s<sup>-1</sup>: (a) the first five cycles in a wide potential range; (b) the two small cathodic peaks appeared in the first scan; (c) the redox peaks for Mg/Mg<sup>2+</sup> in the subsequent (second to fifth) cycles; and (d) the redox peaks for Li/Li<sup>+</sup> in the potential range -0.1 to 0.2 V ( $\Delta E_p=100$  mV).

Before studying the electrochemical properties of Li–Mg alloy electrodes, it is necessary to evaluate the electrochemical behavior of pure magnesium metal. Shown in Figs. 4 and 5 are the CVs of a pure Mg electrode in 1 M LiN(-SO<sub>2</sub>CF<sub>3</sub>)<sub>2</sub>-EC/DMC (1:2 by vol.) at a scan rate of 1 mV s<sup>-1</sup> over two different potential ranges. The potential was swept from the open circuit voltage (OCV), 2.2 V versus Li<sup>+</sup>/Li, in the cathodic direction down to the set limit and then in the anodic direction. When the potential was scanned from 2.2 to -0.1 V, we found two very small cathodic peaks in the potential range between OCV and 0.4 V in the first cycle (Fig. 4(b)). The cathodic current then increased dramatically

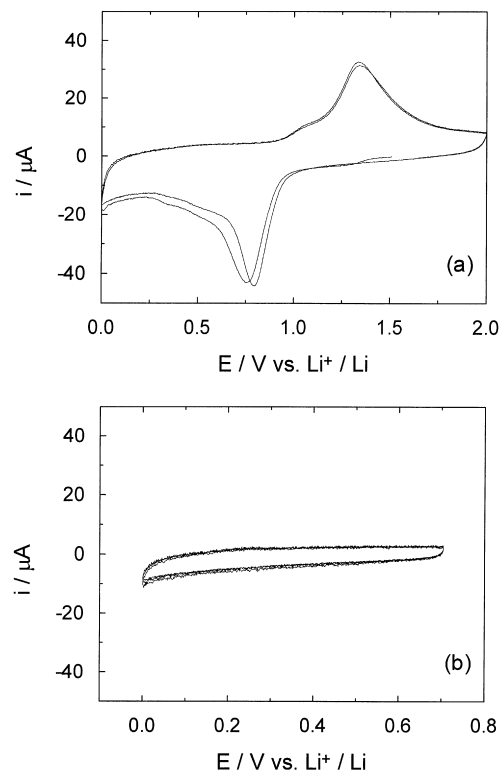


Fig. 5. Cyclic voltammograms of a pure Mg electrode in 1 M LiN(CF<sub>3</sub>SO<sub>2</sub>)<sub>2</sub>-EC/DMC (1:2 by vol.) with a scan rate of 1 mV s<sup>-1</sup> in the potential range of (a) 2.2–0 V ( $\Delta E_p=560$  mV); and (b) 0.7–0 V.

when the potential was below 0 V, corresponding to deposition of Li on the electrode. In the anodic direction, we observed a large peak around 0.08 V and a small peak around 1.35 V. After the first cycle, we observed only one cathodic peak at 0.85 V in subsequent cycles, as shown in Fig. 4(c). The peak current was found to increase during the first three cycles and stabilize thereafter. The anodic peak current around 1.35 V increased from 18 to 30  $\mu$ A during the first two cycles and then stabilized at 30  $\mu$ A. The pair of redox peaks at 1.35 and 0.85 V correspond to the oxidation of Mg and reduction of Mg<sup>2+</sup>; i.e. the redox process of



This is further confirmed by the fact that there was only one pair of redox peaks when the potential scan range was restricted between 2 and 0 V (Fig. 5(a)). Since there are no Mg<sup>2+</sup> ions in the electrolyte solution at the beginning of the experiment, the two small cathodic current peaks in the first negative scan must have resulted from the reduction of a small amount of impurity metal ions; these two small peaks disappeared in subsequent cycling. After the first anodic scan, Mg metal is oxidized to Mg<sup>2+</sup> ions, and therefore, the reduction peak for the Mg<sup>2+</sup> ions increased in following cycles. The remaining pair of redox peaks between 0.1 and -0.1 V correspond to the process of deposition/oxidation (dissolution) of lithium onto/from the Mg electrode surface. The observed peak separation and the rate of current change

indicate that the kinetics of deposition/dissolution of lithium onto/from the Mg electrode is very fast ( $\Delta E_{p, Li} = 100$  mV), but that the kinetics of the oxidation/reduction of Mg (Eq. (1)) is slow ( $\Delta E_{p, Mg} = 560$  mV). As expected, when the potential was scanned between 0.7 and 0 V, we observed no redox peak in the CVs (Fig. 5(b)), indicating that there was no oxidation or reduction processes occurring in this range.

### 3.2. Electrochemical behavior of Li–Mg alloy electrodes prepared by direct-alloying

Shown in Fig. 6 are cyclic voltammograms for different composition Li–Mg alloys prepared by the direct-alloying method. Here, we display the first five cycles in the range from 0.7 to 0 V. It is interesting to note that no matter what

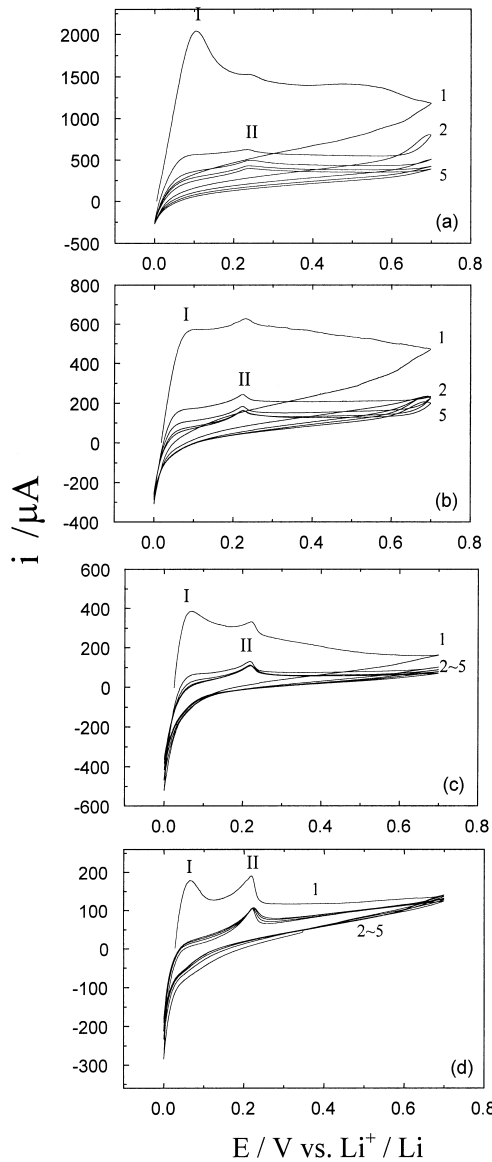


Fig. 6. Cyclic voltammograms of  $Li_xMg_{1-x}$  alloy electrodes (via direct-alloying) in 1 M  $LiN(CF_3SO_2)_2$ -EC/DMC (1:2 by vol.) with a scan rate of  $1 \text{ mV s}^{-1}$ : (a)  $x=0.9$ ; (b)  $x=0.8$ ; (c)  $x=0.7$ ; and (d)  $x=0.6$ .

the composition of the Li–Mg alloy, there appears an oxidation peak around 0.08 V (peak I) in the first anodic scan. This oxidation peak decreased quickly during following cycles and finally disappeared. In contrast, the oxidation peak close to 0.24 V (peak II) in these CVs, appeared in all cycles and became the only oxidation peak observed after several cycles. The cyclic voltammograms of the first cycle are very different from those of the following cycles for all of the Li–Mg alloy compositions tested. Obviously, these two oxidation peaks are not due to the oxidation of Mg (Fig. 5(b)). In order to assess the processes occurring at these two potentials, additional experiments were carried out with a  $Li_7Mg_3$  alloy.

Shown in Fig. 7 are a series of cyclic voltammograms for the  $Li_7Mg_3$  alloy electrode at different negative potential

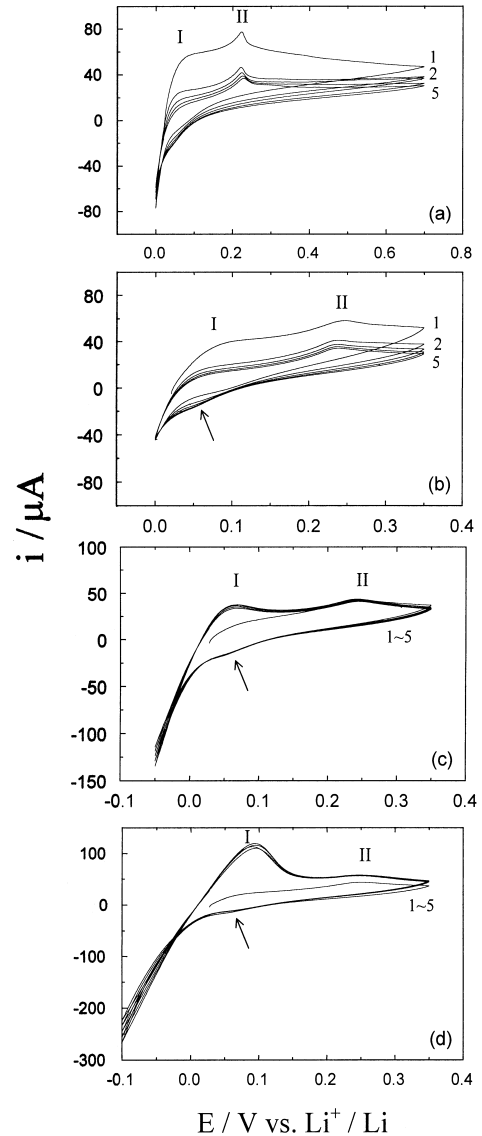


Fig. 7. Cyclic voltammograms of a  $Li_7Mg_3$  electrode (via direct-alloying) in 1 M  $LiN(CF_3SO_2)_2$ -EC/DMC (1:2 by vol.) with a scan rate of  $1 \text{ mV s}^{-1}$  in the potential range of (a) 0.7–0 V; (b) 0.35–0 V; (c) 0.35 to  $-0.05$  V; and (d) 0.35 to  $-0.10$  V.

limits (all upper limits were the same at 0.35 V). When the negative potential limit shifts from 0 to  $-0.05$  V and then to  $-0.1$  V, the peak current for peak I increases dramatically whereas the current for peak II remains almost unchanged. The cathodic current also increases dramatically when the potential limit becomes negative. If we combine these results with our observations on the pure Mg electrode (Figs. 4 and 5), it can be concluded that peak I (at 0.08 V) corresponds to the stripping of pure Li at the Li–Mg alloy surface and peak II (at 0.24 V) corresponds to the extraction of Li atoms from the Li–Mg alloy electrodes. Careful analysis of the CVs in Fig. 7 indicates that there is a very small cathodic peak around 0.05 V. This cathodic peak corresponds to the insertion of Li into the Li–Mg alloy. The alloying and de-alloying processes are kinetically slow. It is interesting to note that when the limit for the potential scan in the negative direction was set at 0 V (Fig. 7(a) and (b)), the anodic peak (peak I and peak II) currents decreased with cycling, as is also observed in Fig. 6. When the limit for the potential scan was shifted to  $-0.05$  V (Fig. 7(c)), the cathodic and anodic currents remained relatively constant for the first five cycles, in stark contrast to those observed on a Pt or a Mg electrode (Figs. 3 and 4), indicating that the tendency for dendrite formation is highly suppressed on the Li–Mg alloy electrode. Still further, when the potential limit is shifted to  $-0.1$  V (Fig. 7(d)), the changes in peak currents are small during cycling.

Since the Li–Mg alloys were prepared at temperatures above  $650^{\circ}\text{C}$  under vacuum, Li metal must vaporize under such conditions (the melting point of lithium is  $179^{\circ}\text{C}$ ). As the stainless-steel containment vessel cools to room temperature, the lithium vapor will condense onto the alloy surface, leaving a thin coating of pure lithium on this surface. During the first anodic scan, this lithium coating will be oxidized to  $\text{Li}^+$  ions, producing a large anodic current peak at 0.08 V, as we observe in Fig. 6. This anodic current decreases when the lithium composition in alloy is reduced from 90 to 60 mol%. At a scanning potential above 0 V, no  $\text{Li}^+$  ions could be reduced to Li metal; there was no corresponding cathodic peak in the negative scan as the anodic current decreased very rapidly. As the Li–Mg alloy becomes more magnesium-rich, the lithium insertion and extraction processes become dominant; peak II was the only oxidation peak after one or two cycles when the alloy, with a composition of  $\text{Li}_7\text{Mg}_3$  or  $\text{Li}_6\text{Mg}_4$ , was used (Fig. 6(c) and (d)).

It is also observed that the height of the anodic peak current changed during cycling, due possibly to changes in Li content in the alloy. Some of the Li may diffuse into the alloy and thus be trapped.

### 3.3. Diffusion coefficient of Li in Li–Mg alloys

As discussed earlier, in order to reduce the formation of lithium dendrites during charging, the microstructure of the electrode must facilitate the efficient transport of lithium

away from the electrode–electrolyte interface into the alloy at a sufficiently fast rate. The factor that controls this process is the diffusion of lithium in alloy. It is well known that the diffusion process for Li atoms in a Li alloy is the rate-determining step when Li atoms intercalate into alloy. Therefore, it is important to determine the lithium diffusion coefficient in these alloys. A potentiostatic transient method, chrono-amperometry, was used to determine the diffusion coefficient of Li atoms in the solid Li–Mg alloys [11–13].

When the potential is stepped from OCV to a value sufficiently positive (e.g. 0.65 V) so that the overall response is controlled by the extraction of Li from the Li–Mg alloy, the diffusion process inside the solid alloy, the observed current is described by the Cottrell equation [11–13]

$$I(t) = zFS(c_{\text{Li}}^* - c_{\text{Li}}) \sqrt{\frac{D_{\text{Li}}}{\pi t}} \quad (2)$$

here  $z$  is the charge number of the electroactive species (Li atoms) in the electrolyte phase,  $F$  the Faraday constant,  $S$  the active surface area of the electrode,  $D_{\text{Li}}$  the diffusion coefficient of Li in the Li–Mg electrode,  $c_{\text{Li}}$  is the lithium concentration at the surface of the Li–Mg alloy electrode, and  $c_{\text{Li}}^*$  is the initial uniform concentration of Li in the alloy.

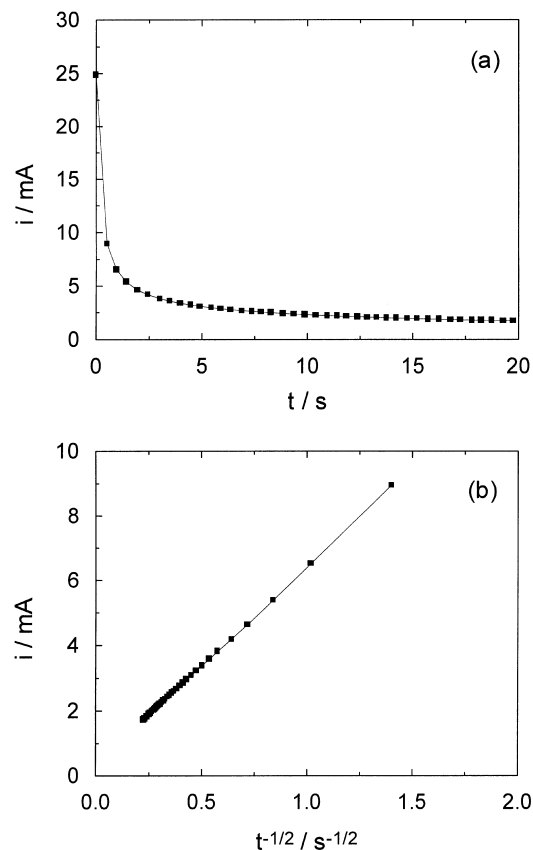


Fig. 8. (a) A typical chronoamperogram of a  $\text{Li}_6\text{Mg}_4$  alloy electrode in 1 M  $\text{LiN}(\text{CF}_3\text{SO}_2)_2\text{-EC/DMC}$  (1:2 by vol.). The potential was stepped from  $\text{OCV} = -0.026$  to 0.65 V (vs.  $\text{Li}^+/\text{Li}$ ), and kept at 0.65 V for 20 s; (b) Cottrell relationship,  $I \sim t^{-1/2}$ , based the data shown in Fig. 8(a).

Table 2  
Diffusion coefficients of lithium in Li–Mg alloys prepared by the direct-alloying method

Composition (Li/Mg)	Diffusivity ( $10^{-8} \text{ cm}^2 \text{ s}^{-1}$ )
90/10	9.89
80/20	5.06
70/30	3.95
60/40	2.46

The diffusion coefficient,  $D_{\text{Li}}$ , can be determined from the slope of a linear plot of  $I$  versus  $t^{-1/2}$ .

A typical chronoamperogram ( $I$  versus  $t$ ) for a  $\text{Li}_6\text{Mg}_4$  alloy is shown in Fig. 8(a) and the relationship between  $I$  and  $t^{-1/2}$  is shown in Fig. 8(b). Listed in Table 2 are the diffusion coefficients for lithium atoms in these Li–Mg alloys as determined from the slope of  $I$  versus  $t^{-1/2}$ . The observed diffusion coefficients increased linearly with the content of lithium in alloy, indicating that the diffusion of Li atoms in the  $\beta$ -Li–Mg phase is relatively sensitive to composition. It should be noted here that all potential step experiments were carried out after the first CV cycle to minimize the effect of the thin lithium coating on the alloys.

### 3.4. Microstructure and surface morphology of Li–Mg alloys prepared by KCVD

The composition, microstructure, and morphology of Li–Mg alloy films produced by the KCVD method under different preparation conditions were systematically studied through independent variation of the temperature of the Mg and Li metal, and of the Li–Mg alloy deposition substrate [5]. The content of Li in the Li–Mg alloy film can be changed from 0.08 to 30 wt.% when the temperature of the Li is varied from  $\sim 405$  to  $535^\circ\text{C}$  and the temperature of Mg from  $\sim 445$  to  $485^\circ\text{C}$ , depending on the precise configuration of the device used to carry out the deposition process. Generally, the higher the temperature of the Li metal, the larger the content of Li in the alloy film. The microstructure and morphology of the alloy films are mainly determined by the substrate temperature. As the substrate temperature is lowered, the microstructure of the deposited film can be made to transform from the cubic crystalline structure characteristic of a phase-equilibrated Li–Mg alloy (with  $>26$  wt.% Li) to a fibrous columnar microstructure and, on further cooling, to a tapered columnar microstructure with extensive voids [5]. The film thus transforms from

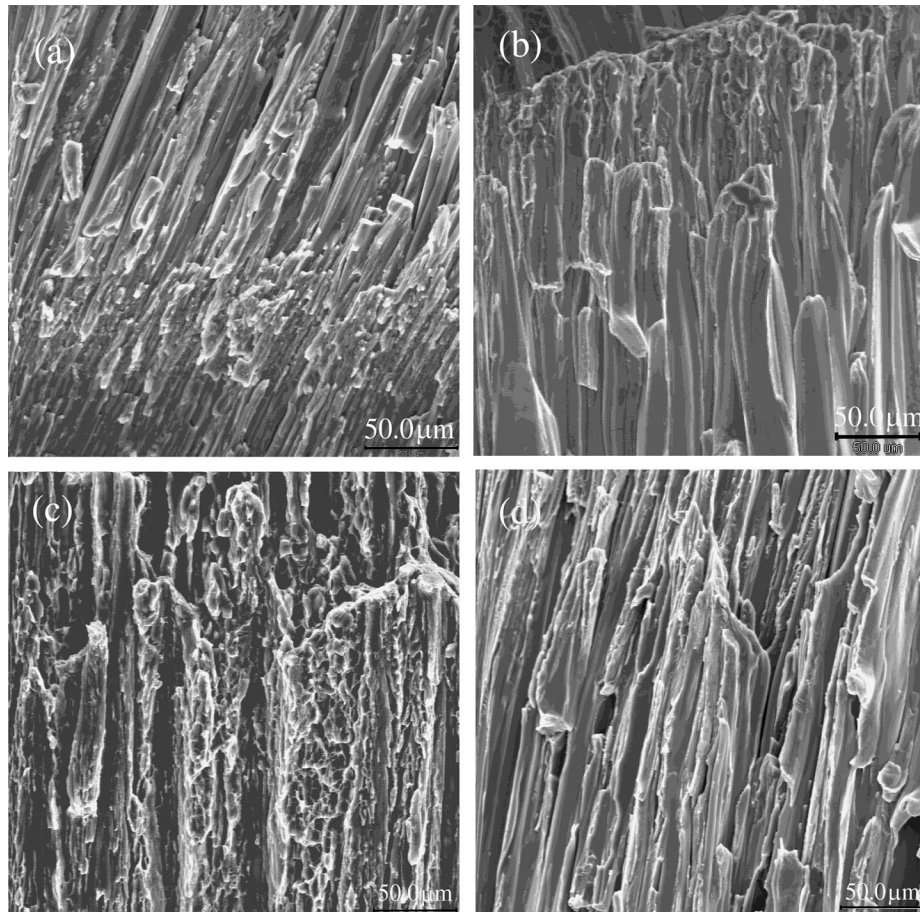


Fig. 9. SEM micrograph of cross-sectional views of Li–Mg alloys prepared by the KCVD under the conditions as specified in Table 1: (a) Sample 1; (b) Sample 2; (c) Sample 3; and (d) Sample 4.

a dense to porous structure. For applications related to lithium batteries, this porous structure is preferred. In addition, based on the experience which we have acquired in handling directly formed Li–Mg alloys, we find that their hardness increases with the content of Mg in the alloy. A high Mg content in excess of 40 mol% (~70 wt.%) renders the alloy too hard to manipulate. It is, therefore, necessary to produce higher Li content Li–Mg alloy films with the corresponding porous structure and we chose the preparation conditions for the Li–Mg alloy films at sufficiently high lithium temperatures and low substrate temperatures (Table 1).

The scanning electron micrographs shown in Fig. 9 correspond to a cross-sectional view of four Li–Mg alloy samples deposited on a Ta substrate at ~30 and 15°C, respectively. All of the samples display a columnar and porous structure. This, of course, is beneficial to the passage of liquid electrolyte into the pores, thereby, increasing the real contact area between the liquid electrolyte and the Li–Mg alloy electrode surface as the alloy film is used as an anode in lithium batteries. Specifically under select conditions (e.g. Li temperature 650°C, Mg temperature 460°C, and Ta substrate temperature 15°C), the obtained alloy

(Sample 4) possesses a substantially porous structure (Fig. 9(d)). In fact, the SEM micrographs taken in top-view demonstrate that the morphology of the deposited alloy films varies significantly as a function of substrate temperature (Fig. 10). When the substrate temperature is 30°C, the surface of the alloy film appears to be relatively dense, displaying a block-like structure (Fig. 10(a) and (b)). A striking change in the surface morphology of the alloy films (Fig. 10(c) and (d)), is apparent at the lower substrate temperature, 15°C, as dry ice cooling is used to adjust the temperature of the substrate. These latter samples consist of highly porous surfaces constituted by fine particles. They clearly have a large real surface area that can facilitate the transport of liquid electrolyte into the Li–Mg alloy electrode.

### 3.5. Electrochemical properties of Li–Mg alloys prepared by KCVD

Shown in Fig. 11 are the cyclic voltammograms of the Li–Mg alloys prepared by the KCVD method under the conditions given in Table 1. Although an anodic peak near 0.22 V appears on all of the CV curves, corresponding to the extraction of Li from the Li–Mg alloys, there are notable

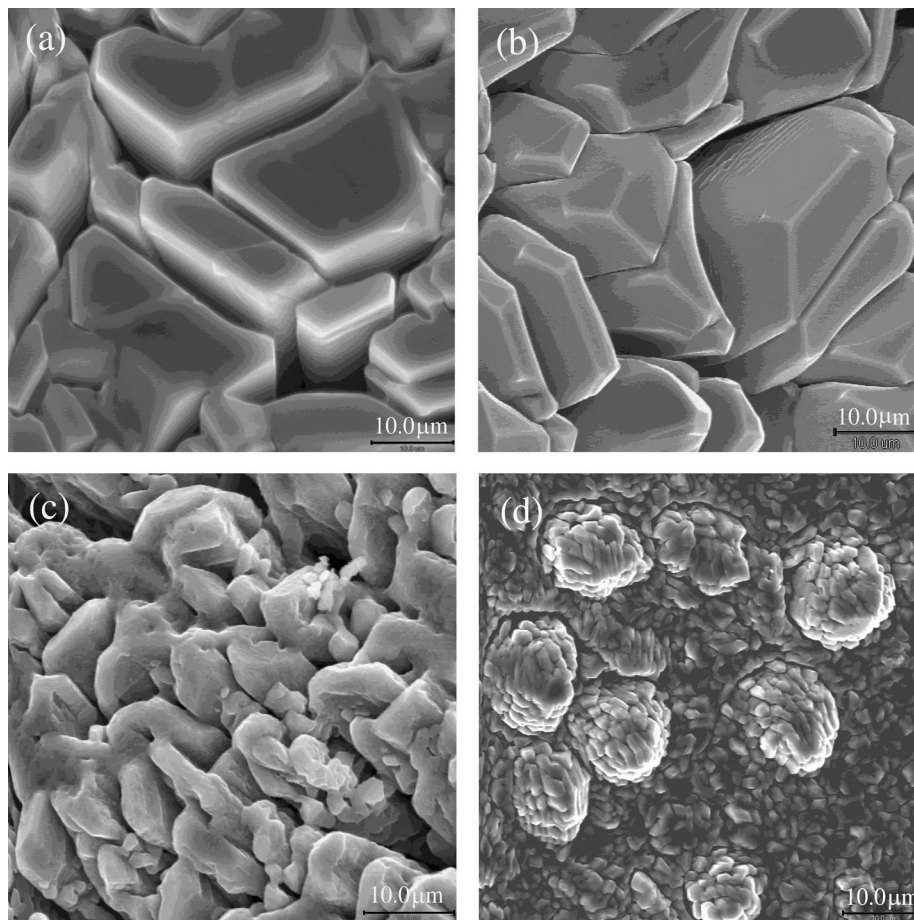


Fig. 10. SEM micrograph of top view of the Li–Mg alloys prepared by the KCVD under conditions as specified in Table 1: (a) Sample 1; (b) Sample 2; (c) Sample 3; and (d) Sample 4.

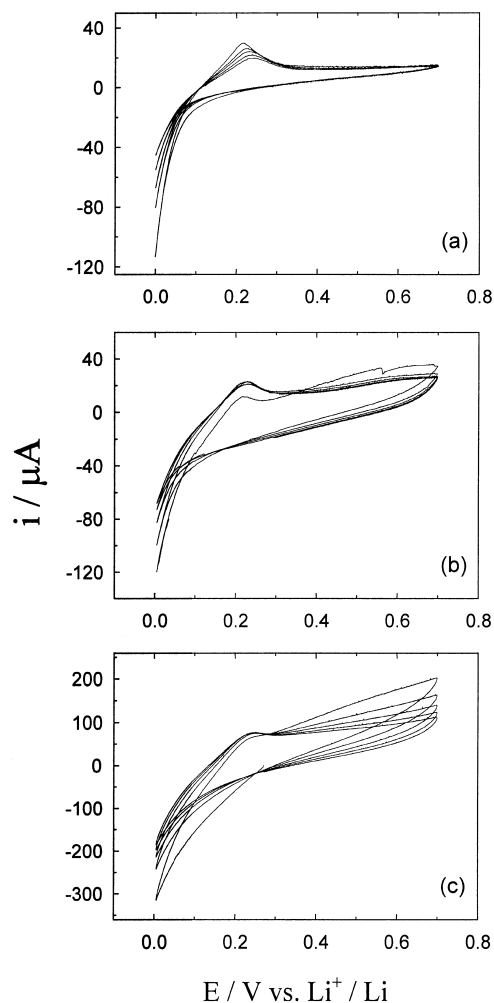


Fig. 11. Cyclic voltammograms of Li–Mg alloy electrodes (generated via KCVD method) in 1 M  $\text{LiN}(\text{CF}_3\text{SO}_2)_2\text{-EC/DMC}$  (1:2 by vol.) with a scan rate of  $1 \text{ mV s}^{-1}$ : (a) Sample 1; (b) Sample 3; and (c) Sample 4.

differences among these CV curves. For Sample 1, the anodic peak current decreased gradually as the anodic peak potential shifted in the positive direction with cycling; the cathodic current decreased quickly. In contrast, for Samples 2–4, the anodic peak current and peak potential remained relatively constant after the first cycle. However, for samples prepared at increasing lithium temperature and decreasing magnesium temperature, the height of the anodic peak current continually reduced, implying a dependence on the composition of the prepared Li–Mg alloys. A similar trend was also observed in studying the Li–Mg alloy films (Fig. 6) prepared using the direct-alloying method; the height of the anodic peak current decreased when the Li content in the alloys was reduced from 90 to 60 mol%. Since the Li–Mg alloy prepared by KCVD at higher Li temperature and lower Mg temperature contains a larger Li concentration, the observation is consistent with previous results (Fig. 6).

The major difference between the CV curves of the KCVD prepared Li–Mg alloys and those prepared by the

direct-alloying method is manifest in the first cycle. A large anodic peak around 0.08 V did not appear in the CV curves for the KCVD prepared Li–Mg alloys, indicating that there is no lithium layer on the surface of the KCVD prepared alloys and that the Li vapor has intimately mixed with the Mg vapor under these preparation conditions. Shown in Table 1 are the values of  $D_{\text{Li}}$  for the KCVD generated Li–Mg alloys, as determined using chronoamperometry. It is noted that the  $D_{\text{Li}}$  values are influenced by the substrate temperature, in other words, by the microstructure and morphology of the Li–Mg alloy electrodes. The more porous the electrodes, the higher the value of  $D_{\text{Li}}$ . The high diffusivity of lithium in these Li–Mg alloys ( $D_{\text{Li}}=1.22 \times 10^{-7}$  to  $5.9 \times 10^{-7} \text{ cm}^2 \text{ s}^{-1}$ ) should be coupled with a significantly enhanced surface diffusion due to the highly porous structures depicted in Figs. 9 and 10. As a result, the diffusion of lithium in these alloys should be sufficiently fast so that the activity of lithium at the electrode interface will remain less than unity. This suggests that these Li–Mg alloy electrodes can be charged or discharged at a higher rate without formation of dendrite, and hence, that lithium batteries based on lithium alloy electrodes will have a higher power density.

#### 4. Conclusions

The observed electrochemical behaviors of Li–Mg alloys, prepared using either direct-alloying or kinetically-controlled vapor deposition, indicate that the tendency for Li dendrite formation is significantly reduced on a Li–Mg alloy electrode. The determined diffusivity of lithium in the Li–Mg alloys, especially those prepared by the KCVD method, is much greater than those of other intercalation electrode materials. It appears that the KCVD process is a useful alloy generating technique; it has the ability to modify the microstructure and morphology of alloy electrodes through substrate temperature control. Not only might the Li–Mg system, whose morphology can be modified through generation on a substrate at room or even lower temperature, provide a means to obviate the problem of lithium dendrite formation during cycling, but also, the high capacity inherent to a lithium alloy electrode ( $642 \text{ mA g}^{-1}$  when it is cycled from  $\text{Li}_4\text{Mg}_6$  to  $\text{Li}_6\text{Mg}_4$ ) might considerably exceed that of currently accessible lithiated carbon electrodes. The long-term reversibility of this high-capacity electrode, however, is still under investigation and will be reported in subsequent communications.

#### Acknowledgements

The authors wish to gratefully acknowledge the financial support of this work by CALEB Corporation and the donors of the Petroleum Research Fund, administered by the American Chemical Society (PRF # 32792-AC5).

## References

- [1] D. Guyomard, T.M. Tarascon, *J. Electrochem. Soc.* 139 (1992) 937.
- [2] J. Wang, I.D. Raistrick, R.A. Huggins, *J. Electrochem. Soc.* 133 (1986) 457.
- [3] D.B. Williams, J.W. Edington, *Met. Sci.* 9 (1975) 529.
- [4] A.J. McAlister, *Bull. Alloy Phase Diagrams* 3 (2) (1982).
- [5] F. Dudel, J.L. Gole, T.A. Sanders, J. King, R.F. Browner, *Philos. Mag. B* 75 (5) (1997) 733–755.
- [6] A.A. Nayeb-Hashemi, A.D. Pelton, J.B. Clark, *Binary Alloy Phase Diagrams* 2 (1984) 1487.
- [7] A. Anani, R. Huggins, *J. Power Sources* 38 (1992) 351–362.
- [8] A. Anani, R. Huggins, *J. Power Sources* 38 (1992) 363–372.
- [9] Y. Iwodate, M. Lassouani, F. Lantelme, M. Chemia, *J. Appl. Electrochem.* 17 (1987) 385–397.
- [10] H.F. Baumann, J.E. Shilton, W.J. Conner, G.M. Cook, Technical Documentary Report No. RTD-TDR-63-4083, Air Force Contract AF 33 (616) 7957, Task No. 817 304, Project No. 8173, AD 425 876. Lockheed Missiles and Space Co., Palo Alto, CA, October 1963.
- [11] C.J. Wen, C. Ho, B.A. Boukamp, I.D. Raistrick, W. Weppner, R.A. Huggins, *Int. Met. Rev.* 5 (1981) 253–268.
- [12] S. Machill, D. Rahner, *J. Power Sources* 54 (1995) 428–432.
- [13] S. Machill, D. Rahner, *J. Power Sources* 68 (1997) 506–509.
- [14] L.F. Mondolfo, *Aluminum Alloys*, Butterworths, London, 1976.
- [15] I. Epelboin, M. Froment, M. Garreau, J. Thevenin, D. Warin, *J. Electrochem. Soc.* 127 (1980) 2100.